Journal of Virology®

AMERICAN SOCIETY FOR MICROBIOLOGY

# Interferon-Inducible GTPase 1 Impedes the Dimerization of Rabies Virus Phosphoprotein and Restricts Viral Replication

Bin Tian,[a,b,c] Yueming Yuan,[a,b,c] Yu Yang,[a,b,c] Zhaochen Luo,[a,b,c] Baokun Sui,[a,b,c] Ming Zhou,[a,b,c] Zhen F. Fu,[a,b,c,d] Ling Zhao[a,b,c]

[a]State Key Laboratory of Agricultural Microbiology, Huazhong Agricultural University, Wuhan, China
[b]Key Laboratory of Preventive Veterinary Medicine of Hubei Province, Huazhong Agricultural University, Wuhan, China
[c]College of Veterinary Medicine, Huazhong Agricultural University, Wuhan, China
[d]Department of Pathology, University of Georgia, Athens, Georgia, USA

Bin Tian and Yueming Yuan contributed equally to this work. Author order was determined alphabetically.

**ABSTRACT** Rabies, caused by rabies virus (RABV), is an ancient zoonosis and still a major public health problem for humans, especially in developing countries. RABV can be recognized by specific innate recognition receptors, resulting in the production of hundreds of interferon-stimulated genes (ISGs), which can inhibit viral replication at different stages. Interferon-inducible GTPase 1 (IIGP1) is a mouse-specific ISG and belongs to the immunity-related GTPases (IRGs) family. IIGP is reported to constrain intracellular parasite infection by disrupting the parasitophorous vacuole membrane. However, the role of IIGP1 in restricting viral replication has not been reported. In this present study, we found that IIGP1 was upregulated in cells and mouse brains upon RABV infection. Overexpression of IIGP1 limited RABV replication in cell lines and reduced viral pathogenicity in a mouse model. Consistently, deficiency of IIGP1 enhanced RABV replication in different parts of mouse brains. Furthermore, we found that IIGP1 could interact with RABV phosphoprotein (P protein). Mutation and immunoprecipitation analyses revealed that the Y128 site of P protein is critical for its interaction with IIGP1. Further study demonstrated that this interaction impeded the dimerization of P protein and thus suppressed RABV replication. Collectively, our findings for the first reveal a novel role of IIGP1 in restricting a typical neurotropic virus, RABV, which will provide fresh insight into the function of this mouse-specific ISG.

**IMPORTANCE** Interferon and its downstream products, ISGs, are essential in defending against pathogen invasion. One of the ISGs, IIGP1, has been found to constrain intracellular parasite infection by disrupting their vacuole membranes. However, the role of IIGP1 in limiting viral infection is unclear. In this study, we show that infection with a typical neurotropic virus, RABV, can induce upregulation of IIGP1, which, in turn, suppresses RABV by interacting with its phosphoprotein (P protein) and thus blocking the dimerization of P protein. Our study provides the first evidence that IIGP1 functions in limiting viral infection and provides a basis for comprehensive understanding of this important ISG.

**KEYWORDS** IIGP1, P protein, dimerization, rabies virus

Rabies is a fatal encephalitis that causes more than 59,000 human deaths globally every year (1). So far, there is no effective treatment for this disease once symptoms appear. Its causative agent, rabies virus (RABV), is a single-stranded negative-sense RNA virus, belonging to the genus *Lyssavirus* of the family *Rhabdoviridae* (2, 3). It encodes five proteins, nucleoprotein (N), phosphoprotein (P), matrix protein (M), glycoprotein

(G), and a large polymerase (L), in the order 3′-N-P-M-G-L-5′ (4). The Negri body (NB) is the viral transcription and replication factory for many negative-sense RNA viruses, including RABV, which is formed with N, P, and L proteins combined with viral RNA and wrapped by a loose membrane structure (5, 6).

P protein consists of 297 amino acids and exists as a dimer in the cell. Each dimer can bind to free N protein in the cytoplasm and form the N-P complex, which can inhibit nonspecific binding of the newly synthesized N protein to the cellular RNA (7, 8). P protein contains two N protein-binding domains; one domain (residues 268 to 297) binds to N-RNA, and the other (residues 69 to 139) binds to the soluble form of N, called N° (not bound to viral RNA) (8–10). The N-terminal 19 residues of P protein can also bind to L protein to promote polymerase function (11). The crystal structure of P protein from amino acid residues 92 to 131 has been resolved, and four amino acids, F114, W118, I125, and Y128, are recognized to be essential for the dimerization of P protein (12). P protein is not only indispensable for viral transcription and replication, but it also interacts with many cellular factors. P protein can interact with the cytoplasmic dynein light chain (LC8) and assist in retrograde axonal transport of RABV (13, 14). In another study, we found that P protein could interact with the ribosomal protein L9, which translocated from the nucleus to the cytoplasm and thus inhibited the early stage of RABV transcription (15).

The innate immune response is the first line to defend against viral invasion. Viruses are usually recognized through specific pattern recognition receptors (PRRs), including Toll-like receptors (TLRs), RIG-I-like receptors (RLRs), and NOD-like receptors (NLRs) (16). Activation of these molecules leads to the production of chemokines, cytokines, and interferons (IFNs). IFNs induce hundreds of interferon-stimulated genes (ISGs) via the JAK-STAT-interferon regulatory factor 9 (IRF9) signaling pathway (17). So far, several ISGs have been reported to function in inhibiting RABV infection. The interferon-induced promyelocytic leukemia (PML) shows an antiviral effect against RABV that functions based on interacting with P protein and then reorganizing nuclear bodies (18). Interferon-induced protein with tetratricopeptide repeats 2 (IFIT2) was demonstrated to inhibit RABV at the stage of viral replication (19, 20). Recently, it was found that viperin (virus inhibitory protein, endoplasmic reticulum associated, IFN inducible) is upregulated upon RABV infection and exhibits an antiviral function in RAW264.7 cells by reducing cholesterol and sphingomyelin on the cellular membrane (21). Our most recent study found that CH25H could suppress RABV infection by inhibiting viral entry into cells (22).

The IFN-inducible GTPase superfamily comprises four subfamilies according to paralogy and molecular mass: the guanylate-binding proteins (GBP), the immunity-related GTPases (IRG), the myxovirus resistance proteins (Mx) proteins, and the very large inducible GTPases (VLIG) (23). Some of the GTPase family members can be upregulated by bacteria and protozoa infection and modulate the phagocytosis through changes in the surface levels of phagocytic receptors (24). All IRGs are located on the Golgi apparatus or endoplasmic reticulum (ER) in a resting situation, but some IRGs can translocate and disrupt the plasma membrane containing intracellular parasites (25). Interferon-inducible GTPase 1 (IIGP1, also termed Irga6) belongs to the IRG family and is a mouse-specific GTPase, which is located on mouse chromosome 11 and mainly induced by IFN gamma (IFN-$\gamma$) (26). The crystal structure revealed that IIGP1 contains a noncrystallographic dimer required for cooperative GTP hydrolysis and GTP-dependent oligomerization of IIGP1 (27). During the infection of some intracellular parasites, including *Toxoplasma gondii* and *Encephalitozoon cuniculi*, IIGP1 destroys the membrane and forces the wrapped contents of pathogens into the cytoplasm (28, 29). IIGP1 deficiency (IIGP1$^{-/-}$) enhanced the replication and pathogenesis of *T. gondii in vitro* and *in vivo* (28, 30). Recently, in a murine norovirus model, IFN-inducible GTPases (immunity-related GTPases, IRGs, and guanylate-binding proteins [GBPs]) were found to be recruited to the viral replication complex (31). However, there is no evidence that IIGP1 can inhibit virus infection. In this present study, we found that RABV infection upregulates IIGP1 and expression of IIGP1 can efficiently inhibit RABV replication both

*in vitro* and *in vivo*. We further determined that IIGP1 can interact with RABV P protein at the amino acid Y128 and thus impede the dimerization of viral P protein.

## RESULTS

**RABV infection induces upregulation of IIGP1.** To select ISGs induced by RABV infection, we infected mice ($n = 3$) intracranially (i.c.) with a lab-attenuated RABV strain CVS-B2c. At 6 days postinfection (dpi), mouse brains were collected and applied to isobaric tags for relative and absolute quantification (iTRAQ) or for quantitative real-time PCR (qPCR) analysis. From iTRAQ data, 490 upregulated proteins were identified, and the top 20 are listed in Fig. 1A. Among these 20 proteins, IIGP1, ranked 4th, was upregulated around 4-fold post-RABV infection. Since IIGP1 has not been reported to inhibit viral replication, we thus focused on IIGP1 in this following study. To confirm iTRAQ results, we analyzed the mRNA level of IIGP1 and its main inducer, IFN-γ, by qPCR. The results demonstrated that both IIGP1 and IFN-γ were upregulated post-RABV infection (Fig. 1B). At 6 dpi, we harvested cortex and cerebellum and then measured IIGP1 expression by Western blotting. We observed an enhanced level of IIGP1 in the cortex and cerebellum from RABV-infected mice compared with mock-infected mice (Fig. 1C). Also, the expression of IIGP1 in RABV-infected brains was confirmed by immunofluorescence assay (IFA) (Fig. 1D). To further confirm these observations *in vivo*, we infected N2a and BV2 cells with RABV at a multiplicity of infection (MOI) of 0.01 or 1 and then measured the mRNA level of IIGP1 at indicated time points postinfection by using qPCR. We found that RABV induced upregulation of IIGP1 in a time-dependent manner (Fig. 1E and F). Together, these data suggest that RABV infection upregulates IIGP1 both *in vitro* and *in vivo*.

**Overexpression of IIGP1 inhibits RABV replication in cells.** Since IIGP1 could be induced by RABV infection, we expected that IIGP1 played a role during RABV replication. Thus, we overexpressed IIGP1 in HEK-293T (293T) cells by transient transfection and then infected the cells with a lab-attenuated RABV strain CVS-B2c (B2c). The results showed that overexpression of IIGP1 could reduce the virus titers in the cell culture supernatant in a dose-dependent manner (Fig. 2A). Consistently, the protein level of RABV-P protein in 293T cells was reduced with increasing doses of IIGP1 expression measured by Western blotting (Fig. 2B). Additionally, we evaluated the antiviral ability of IIGP1 against a dog-derived wild-type (WT) RABV strain, DRV-Mexico. Both virus titration (Fig. 2C) and Western blotting (Fig. 2D) demonstrated that overexpression of IIGP1 could restrict DRV replication in 293T cells.

To further confirm that IIGP1 can inhibit RABV replication in multiple cell lines and mice, we constructed and rescued a recombinant B2c expressing IIGP1 by inserting IIGP1 into the viral genome, named rB2c-IIGP1 (Fig. 3A). After rescuing rB2c-IIGP1, IFA (Fig. 3B) and Western blotting (Fig. 3C) were employed to confirm the expression of IIGP1 during viral replication in N2a cells. The growth dynamics of rB2c-IIGP1 and the parent virus rB2c were compared in N2a and BV2 (microglia) cells. In both cell lines, rB2c-IIGP1 replicated at a lower titer than rB2c at 3 dpi (Fig. 3D and E). Taken together, these data demonstrate that IIGP1 can restrict the replication of RABV in different cell lines.

**IIGP1 overexpression reduces the pathogenicity of RABV in mice.** To assess the impact of IIGP1 on pathogenesis of RABV *in vivo*, rB2c and rB2c-IIGP1 were inoculated intramuscularly (i.m.) in hind legs ($n = 10$) or intradermally (i.d.) in both ears ($n = 10$) of the mice, and body weight change and survival ratios were monitored daily. Post-i.m. inoculation, body weight loss and survival ratios were comparable between rB2c-infected and rB2c-IIGP1-infected mice (Fig. 4A and B). In contrast, the body weight loss of rB2c-IIGP1-infected mice was significantly lower than that of rB2c-infected mice at day 8 post-i.d. infection (Fig. 4C). Consistently, the survival ratio of rB2c-IIGP1-infected mice was significantly increased compared to rB2c-infected mice (Fig. 4D). These data suggest that IIGP1 reduces the pathogenicity of RABV in mice depending on the infection route.
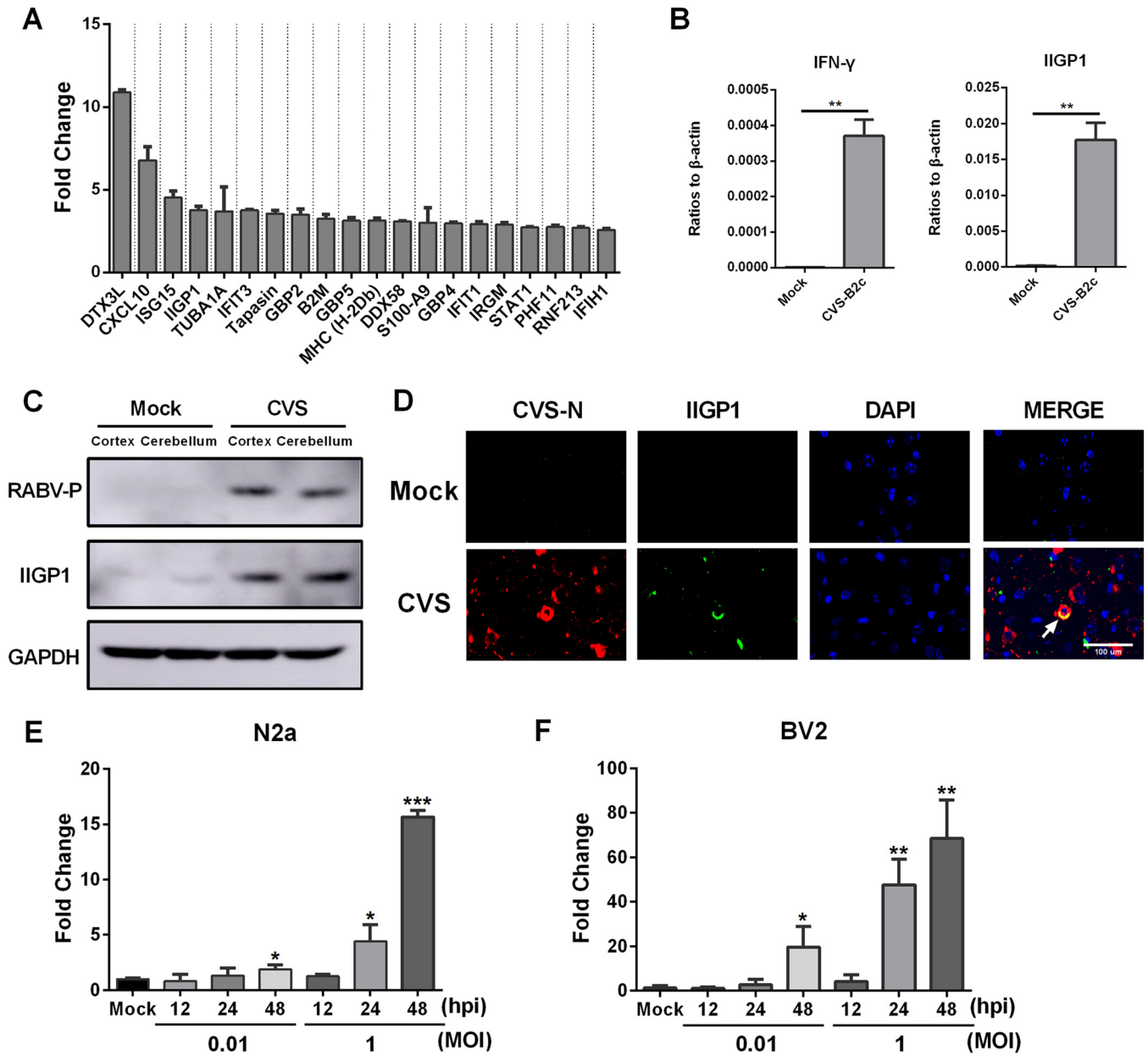
**FIG 1** IIGP1 was upregulated by RABV infection. C57BL/6 mice were i.c. inoculated with RABV CVS-B2c (B2c) at 20 FFU or the same volume of DMEM (mock). At 6 days postinfection (dpi), mouse brains were collected and used for further analysis. (A) The level of proteins in the mouse brain was quantified using iTRAQ, and the top 20 upregulated proteins were selected. The changes of proteins in B2c-infected mouse brains were represented by comparison with the expression level in mock mouse brains ($n = 3$). (B) The total RNA of the brain tissue was isolated, and the mRNA level of IIGP1 and IFN-γ was analyzed by qPCR. (C) The protein level of IIGP1 and RABV-P in the cortex and cerebellum of mouse brains was examined by Western blotting. GAPDH was included as a reference gene. (D) Mouse brains were fixed with 4% paraformaldehyde, paraffin embedded, and sectioned. The IIGP1 expression level was examined by immunofluorescence assay (IFA), and images were taken under a fluorescence microscope. (E and F) N2a cells (E) and BV2 cells (F) were infected with B2c at an MOI of 0.01 and 1 or mock infected. At 12, 24, and 48 h p.i., cells were collected for RNA isolation, and the mRNA level of IIGP1 was analyzed by qPCR ($n = 3$). Error bars represent SD. Statistical differences between viral infected cells and mock were determined by using Student's $t$ test and are denoted as follows: *, $P < 0.05$; **, $P < 0.01$; ***, $P < 0.001$. Scale bar, 100 μm.

Since viral pathogenicity is closely correlated with the virus replication in the brain, we analyzed the viral RNA in different parts of the brain by qPCR post-i.d. inoculation. At 6, 9, and 12 dpi, the olfactory bulb, cortex, cerebellum, and brainstem were collected, and the N mRNA level was quantified by qPCR. The results showed that the viral load in different parts of the brain from rB2c-IIGP1-infected mice was significantly lower than that from rB2c-infected mice at 12 dpi (Fig. 4E to H). These results demonstrate that overexpression of IIGP1 can restrict RABV replication in the brain and reduce the virus pathogenicity.
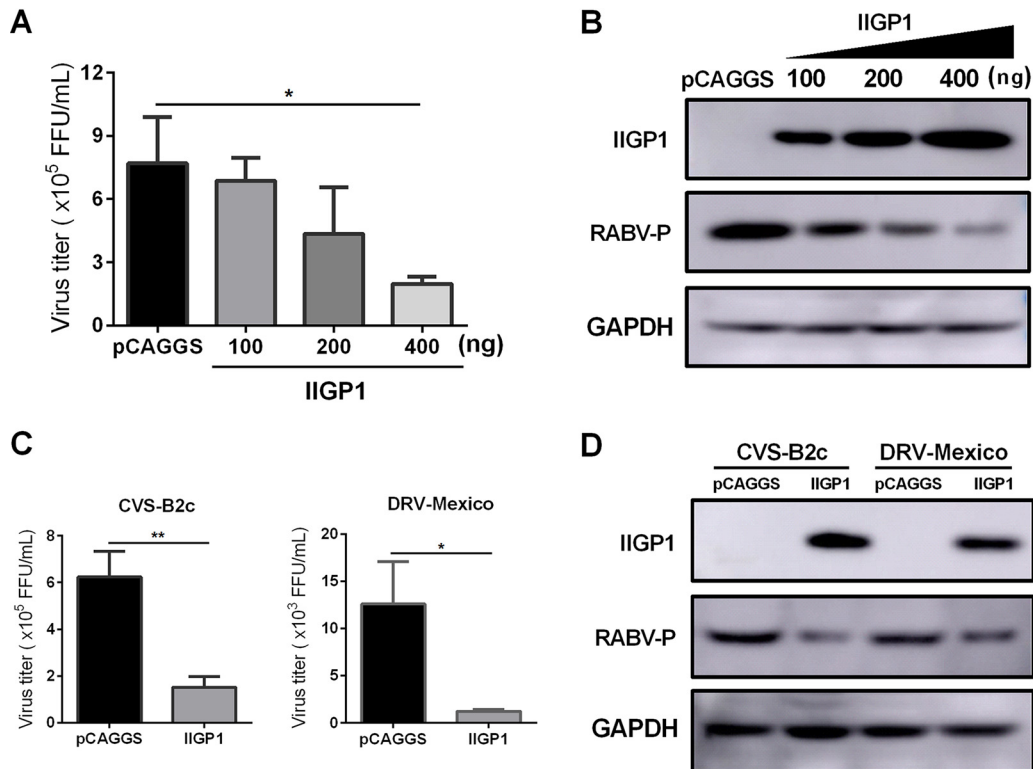
**FIG 2** IIGP1 inhibits RABV replication in cells. Overexpression of IIGP1 decreased the viral titer in cell supernatant and viral protein in cells. 293T cells were transfected with the mammalian expression vector pCAGGS or pCAGGS expressing FLAG-IIGP1 (pC-FLAG-IIGP1) at 100, 200, or 400 ng. At 12 h posttransfection (h p.t.), the cells were infected with B2c at an MOI of 0.01. (A) At 24 h p.i., the culture supernatant of 293T cells was collected, and the viral titer was examined on BSR cells. (B) At 36 h p.i., 293T cells were lysed with radioimmunoprecipitation assay (RIPA) buffer, and the protein levels of IIGP1, RABV-P, and GAPDH were analyzed by Western blotting. (C and D) 293T cells were transfected with pC-FLAG-IIGP1 or pCAGGS. At 12 h posttransfection, the cells were infected with CVS-B2c or DRV-Mexico at an MOI of 0.01. At 36 h p.i., supernatant was collected for virus titration (C), and the cells were harvested for Western blot analysis (D). Error bars represent SD ($n = 3$). Statistical differences were determined by using Student's $t$ test and are denoted as follows: *, $P < 0.05$; **, $P < 0.01$.

**IIGP1 deficiency enhances RABV replication in mouse brains.** To further investigate the role of endogenous IIGP1 in controlling RABV infection, we constructed IIGP1 gene knockout (IIGP1$^{-/-}$) mice utilizing the CRISPR/Cas9 technique, and the successful construction of IIGP1$^{-/-}$ mice was confirmed by PCR genotyping. IIGP1$^{-/-}$ ($n = 10$) and WT ($n = 10$) mice were infected i.m. or i.d. with B2c, and the clinical symptoms were monitored daily. Post-i.m. infection, the survivor ratio between IIGP1$^{-/-}$ and WT mice was comparable ($P = 0.66670$) (Fig. 5A). Similarly, no significant difference for the survivor ratio between IIGP1$^{-/-}$ and WT mice was observed post-i.d. infection ($P = 0.0575$) (Fig. 5B). However, the viral load in the cortex, olfactory bulb, cerebellum, and brain stem from IIGP1$^{-/-}$ mice was significantly higher than that from WT mice at day 6 or 8 post-i.d. infection (Fig. 5C to F). Together, these data illustrate that IIGP1 deficiency enhances RABV replication in mouse brains, suggesting that IIGP1 plays a role in restricting RABV replication in the brain.

**IIGP1 interacts with RABV-P.** To explore the mechanism of how IIGP1 restricts RABV replication, we investigated whether IIGP1 could interact and then interfere with viral protein expression. We inserted IIGP1 fused with a FLAG tag into the mammalian expression vector pCAGGS, resulting in pC-FLAG-IIGP1. Then we transfected this plasmid into 293T cells for 24 h and infected the cells with B2c. At 36 hours postinfection (h p.i.), the whole-cell lysates were collected and added with anti-FLAG tag monoclonal antibody (MAb) to precipitate IIGP1. We found that both N and P proteins of RABV, but not G protein, could be precipitated by IIGP1 (Fig. 6A). Since N and P proteins could
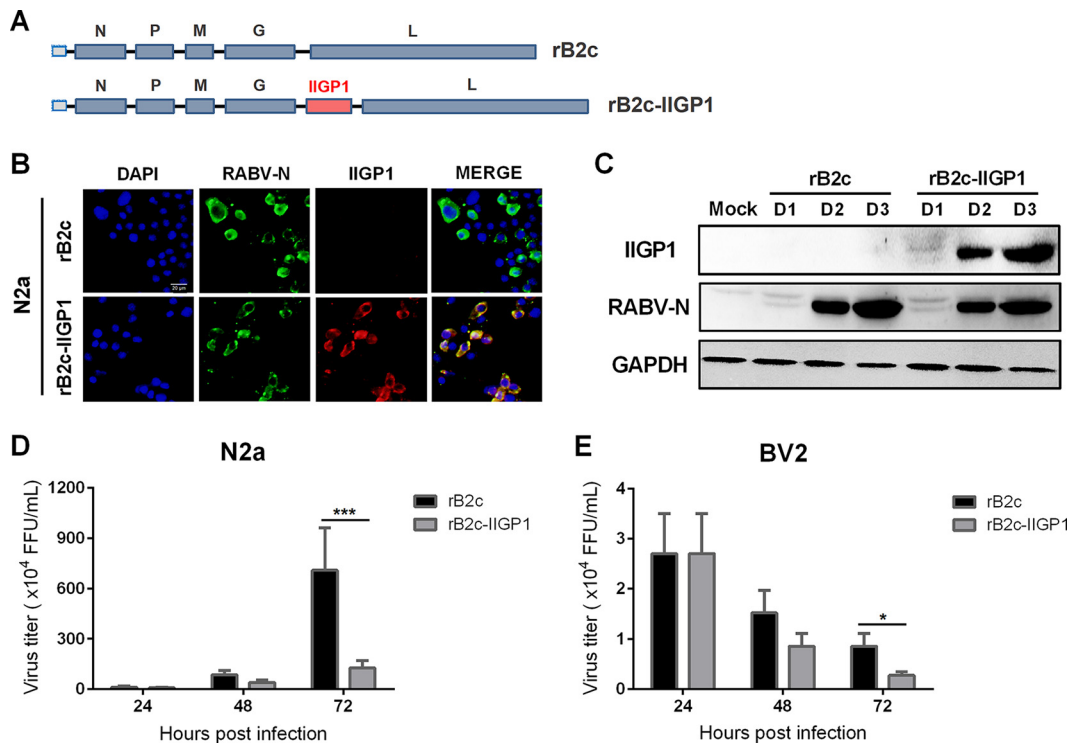
**FIG 3** Construction and characterization of the recombinant RABV expressing IIGP1. (A) Strategies for construction of the full-length cDNA clones of rB2c expressing IIGP1 and rB2c-IIGP1. (B) N2a cells were infected with rB2c-IIGP1 or rB2c at an MOI of 0.01. Cells were fixed at 48 h p.i. and stained with antibodies against RABV-N, IIGP1, or DAPI. Images were taken under a fluorescence microscope. The scale bar represents 20 μm. (C) N2a cells infected with rB2c-IIGP1 or rB2c were harvested using RIPA lysis buffer at 1, 2, and 3 dpi and then subjected to Western blotting. (D and E) N2a and BV2 cells were infected with rB2c-IIGP1 and rB2c at an MOI of 1, and viral titers in cell culture supernatant were measured at the indicated time postinfection (n = 3). The scale bar represents 20 μm. Error bars represent SD.

interact with each other, we expressed N or P protein fused with a hemagglutinin (HA) tag separately and then investigated the interaction between IIGP1 and N/P by immunoprecipitation with anti-HA tag MAb. The result showed that P protein, but not N protein, interacted with IIGP1 (Fig. 6B). To confirm this observation, after expression with IIGP1 and P protein in 293T cells, we precipitated IIGP1 with anti-FLAG-tag MAb and verified the interaction between IIGP1 and P protein (Fig. 6C). We then further confirmed this interaction in N2a cells infected with rB2c or rB2c-IIGP1. At 48 h p.i., we precipitated P protein with anti-P MAb and found that P protein could interact with IIGP1 in rB2c-IIGP1-infected cells (Fig. 6D).

Since we have shown that IIGP1 can restrict both lab-attenuated RABV (CVS-B2c) and WT RABV (DRV-Mexico), we wonder if IIGP1 interacts with the P protein of DRV-Mexico. Immunoprecipitation was employed to confirm the interaction of IIGP1 with P protein of DRV-Mexico (Fig. 6E).

The above studies have proven that the expressed IIGP1 interacts with RABV-P. Next, we wonder if the endogenous IIGP1 induced by RABV infection can also interact with RABV-P. The mouse microglia, BV2 cells, were infected by CVS-B2c (B2c) and DRV-Mexico (DRV), respectively. By using confocal microscopy, we found that both B2c and DRV could induce the expression of IIGP1 in BV2 cells at 36 h p.i. To be noted, B2c induced a higher level of IIGP1 than DRV in BV2 cells, and colocalization of IIGP1 and RABV-P could be observed in B2c- and DRV-infected BV2 cells (Fig. 6F). Together, these data demonstrate that IIGP1 can interact with the P protein of both lab-attenuated and WT RABV strains.

**Y128 of RABV-P determines the interaction between IIGP1 and P protein.** To pinpoint the interaction site of P protein with IIGP1, we truncated P protein of B2c into five fragments, fused with an HA tag in the N terminus, and inserted them into pCAGGS
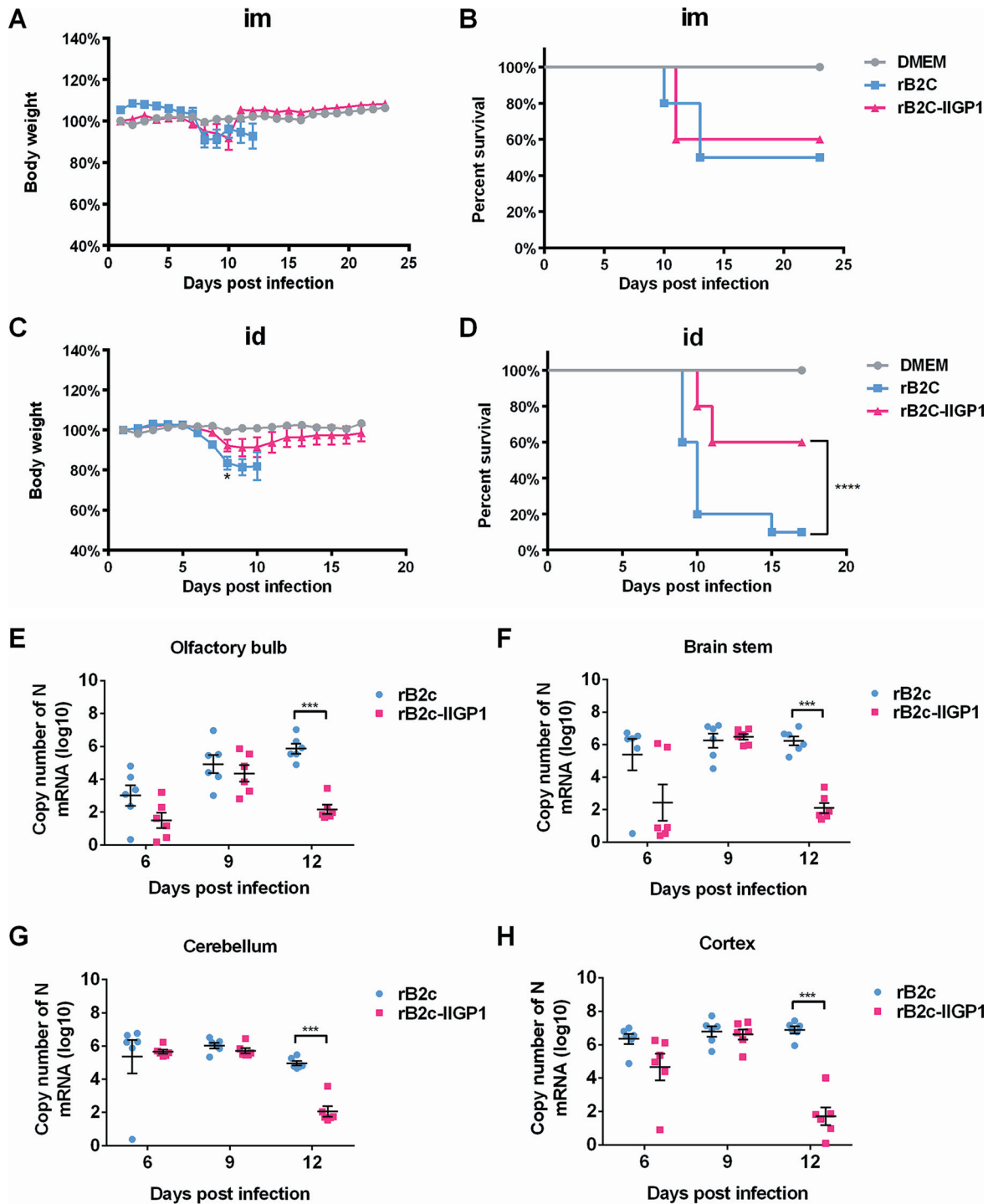
**FIG 4** IIGP1 reduces RABV pathogenicity in mice. Groups of female C57BL/6 mice (8 weeks old, $n = 10$/group) were infected i.m. with DMEM, rB2c, or rB2c-IIGP1 at $6 \times 10^4$ FFU or infected i.d. with rB2c or rB2c-IIGP1 at $6 \times 10^3$ FFU. Then, the body weight change (A and C) and survival ratio (B and D) were monitored for 23 days post-i.m. infection and 17 days post-i.d. infection. Brain tissues from i.d. infection with RABV were collected at 6, 9, and 12 dpi. (E to H) RABV-N mRNA levels in olfactory bulb, cortex, cerebellum, and brain stem were analyzed by qPCR at 6, 9, and 12 dpi ($n = 6$). Error bars represent standard error of mean (SEM). The body weight change was analyzed by two-way ANOVA and Sidak's multiple-comparison test, and survivor ratio was analyzed by Mantel-Cox test (*, $P < 0.05$; ***, $P < 0.001$; ****, $P < 0.0001$).

separately; they were termed pC-HA-P19-297, pC-HA-P52-297, pC-HA-P83-297, pC-HA-P138-297, and pC-HA-P172-297. We then transfected them together with pC-FLAG-IIGP1 and then precipitated IIGP1 by using anti-FLAG tag antibody. After deletion of the P1-82 amino acid (aa), the interaction between IIGP1 and P protein remained; however,
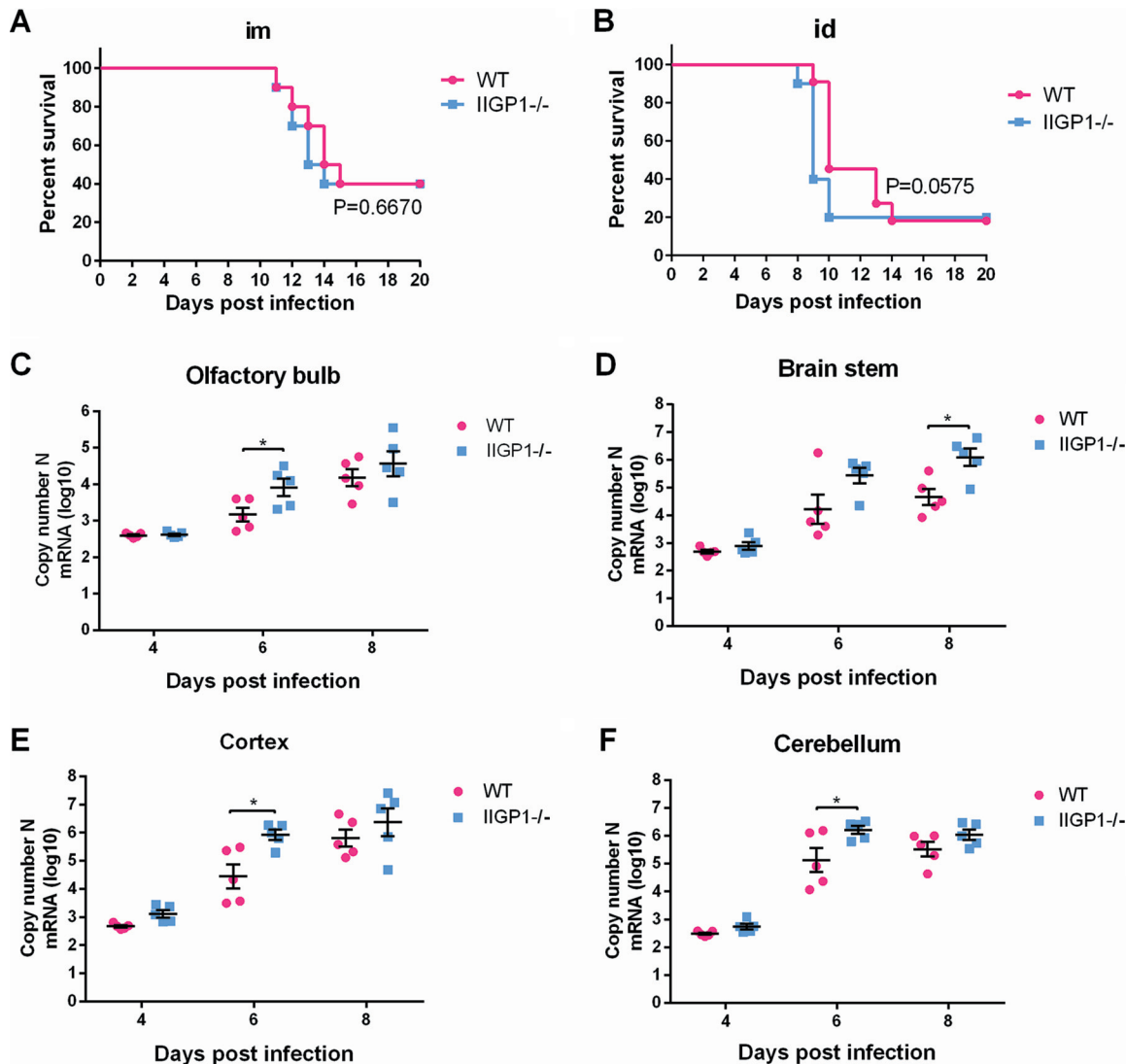
**FIG 5** IIGP1 deficiency increases RABV replication in mouse brains. WT (C57BL/6) and IIGP1 knockout (IIGP1$^{-/-}$) mice (6 weeks old, WT, $n = 10$; IIGP1$^{-/-}$, $n = 10$) were infected i.m. with rB2c at $6 \times 10^4$ FFU or infected i.d. with rB2c at $1.5 \times 10^3$ FFU. The survival ratios of mice post-i.m. infection (A) and i.d. infection (B) were calculated and analyzed by the Gehan-Breslow-Wilcoxon test. (C to F) RABV N mRNA in the olfactory bulb, cortex, cerebellum, and brain stem was analyzed by qPCR at 4, 6, and 8 dpi ($n = 5$). Error bars represent SEM. The survival ratios in panels A and B were analyzed by Gehan-Breslow-Wilcoxon test. The asterisks indicate significant differences between infected WT mice and IIGP1$^{-/-}$ mice at the same time points in panels C to F determined by two-way ANOVA and Sidak's multiple-comparison test. Statistical differences are denoted as follows: *, $P < 0.05$.

this interaction disappeared when P1-137 aa was deleted (Fig. 7A), suggesting that the interaction region between IIGP1 and P protein was located between 83 and 138 aa. To further confirm the interaction sites, we constructed the truncated fragments P1-52, P1-69, P1-83, and P1-138 of P protein fused with an HA-green fluorescent protein (GFP) protein (an HA tag linked in the N terminus of GFP), and the interaction between IIGP1 and P protein truncations was assessed by immunoprecipitation. The fragment HA-GFP-P1-138 interacted with IIGP1 in the same way as the full length of P protein, while HA-GFP-P1-83 lost the interaction with IIGP1 (Fig. 7B), suggesting that the interaction region between IIGP1 and P protein is located between 84 and 138 aa.

We then further constructed five truncated fragments of P protein fused with an HA-GFP protein, P1-97, P1-111, P1-125, P1-129, and P1-132. The results showed that GFP-P1-129 could be precipitated by IIGP1, while GFP-P1-125 could not (Fig. 7C and D). Thus, the interaction region was narrowed down to four amino acids between 125 and 129 aa. We then constructed four HA tag-fused P protein mutants, namely, HA-P V126A,
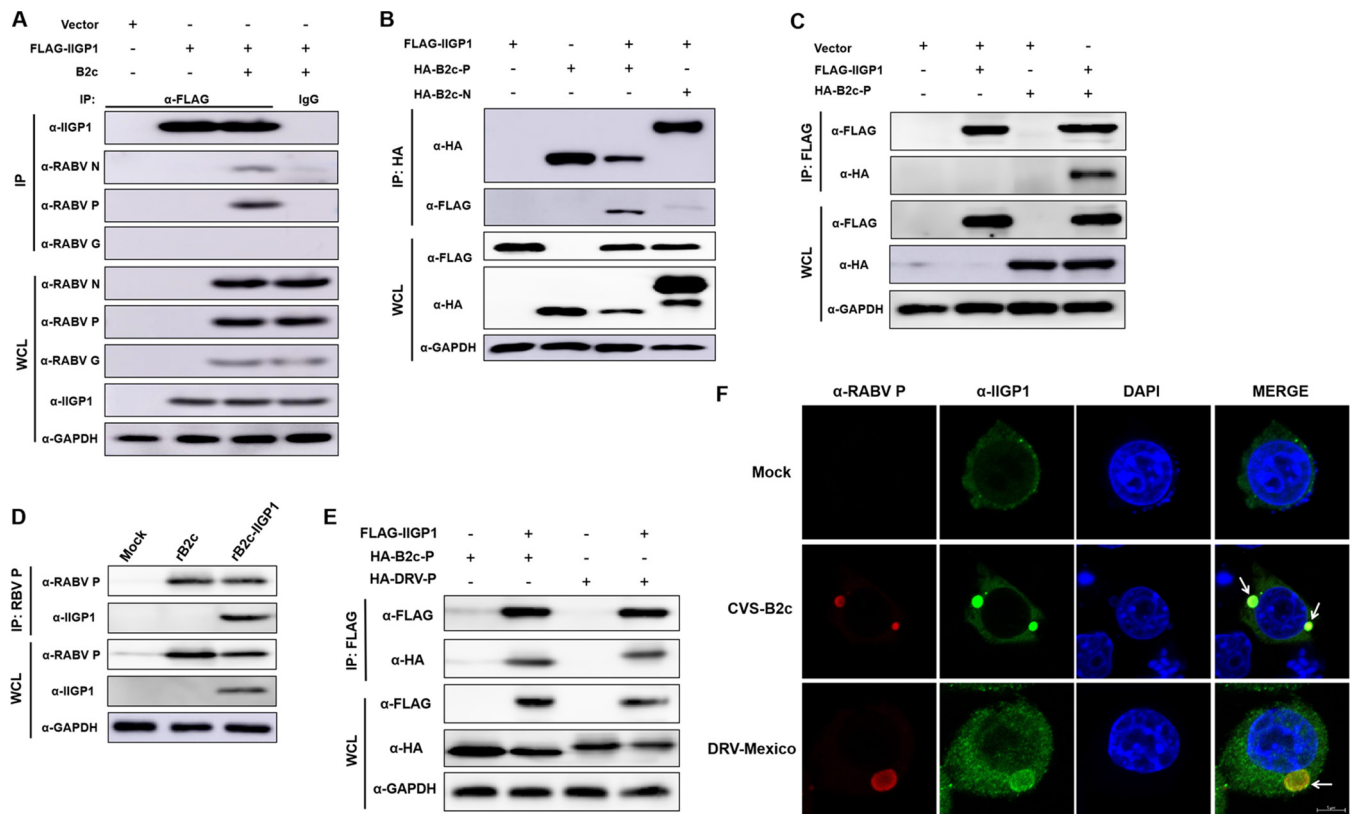
**FIG 6** IIGP1 interacts with RABV-P. (A) 293T cells were transfected with pC-FLAG-IIGP1 or empty vector pCAGGS. At 12 h p.t., cells were infected with B2c at an MOI of 1 and then were lysed with NP-40 lysis buffer at 36 h p.i. Coimmunoprecipitation (co-IP) was executed with MAb against FLAG tag, and IgG was used as the negative control. Western blotting was performed to detect the products from IP and whole-cell lysate (WCL) with the indicated antibodies. (B) 293T cells were cotransfected with pC-FLAG-IIGP1, pC-HA-B2c-P, pC-HA-B2c-N, or pCAGGS. At 48 h p.t., co-IP and Western blotting were performed with the indicated antibodies. (C) 293T cells were cotransfected with pC-FLAG-IIGP1, pC-HA-B2c-P, or pCAGGS. At 48 h p.t., co-IP and Western blotting were performed with the indicated antibodies. (D) N2a cells were infected with rB2c or rB2c-IIGP1 at an MOI of 1. At 48 h p.i., co-IP and Western blotting were performed with the indicated antibodies. (E and F) 293T cells were cotransfected with pC-FLAG-IIGP1, pC-HA-B2c-P, pC-HA-B2c-N, or pCAGGS. At 48 h.p.t., co-IP and Western blotting were performed with the indicated antibodies. (E) BV2 cells were infected with CVS-B2c or DRV-Mexico or mock infected for 36 h, fixed with 4% paraformaldehyde, stained with MAbs against IIGP1, RABV-P, or DAPI, and then observed under a confocal fluorescence microscope (F). The scale bar represents 5 μm.

HA-P S127A, HA-P Y128A, and HA-P V129A. Interestingly, we found that HA-P Y128A almost lost the interaction with IIGP1, while the other three mutations retained the interaction with IIGP1 (Fig. 7E). Moreover, we found that P Y128A of both B2c and DRV-Mexico strains lost the interaction with IIGP1 (Fig. 7F). These data together demonstrate that Y128 of P protein is critical for the interaction between IIGP1 and P protein.

**IIGP1 interferes with the dimerization of RABV-P.** Previous studies reported that the dimerization of P protein was located between 91 and 132 aa, and the dimerization was formed by some hydrophobic bonds (12). At least four amino acids (F114, W118, I125, and Y128) were critical for the dimerization of P protein (12). Here, our results demonstrated that Y128 of P protein determines the interaction between IIGP1 and P protein. Thus, we propose that IIGP1 binding with P protein may interfere with the dimerization of P protein. To confirm this hypothesis, we constructed a V5 tag-fused P protein expression plasmid pC-V5-B2c-P and then transfected it together with pC-HA-B2c-P and pC-FLAG-IIGP1 plasmids in 293T cells. The immunoprecipitation results showed that the P-P interaction was dramatically impaired by increasing doses of IIGP1 expression (Fig. 8A).

To further confirm that IIGP1 disrupts the dimerization of P protein, bimolecular fluorescence complementation (BiFC) was applied to measure the dimerization of P protein. Plasmids pBiFC-VC155-B2c-P and pBiFC-VN155 (I152L)-B2c-P, together with
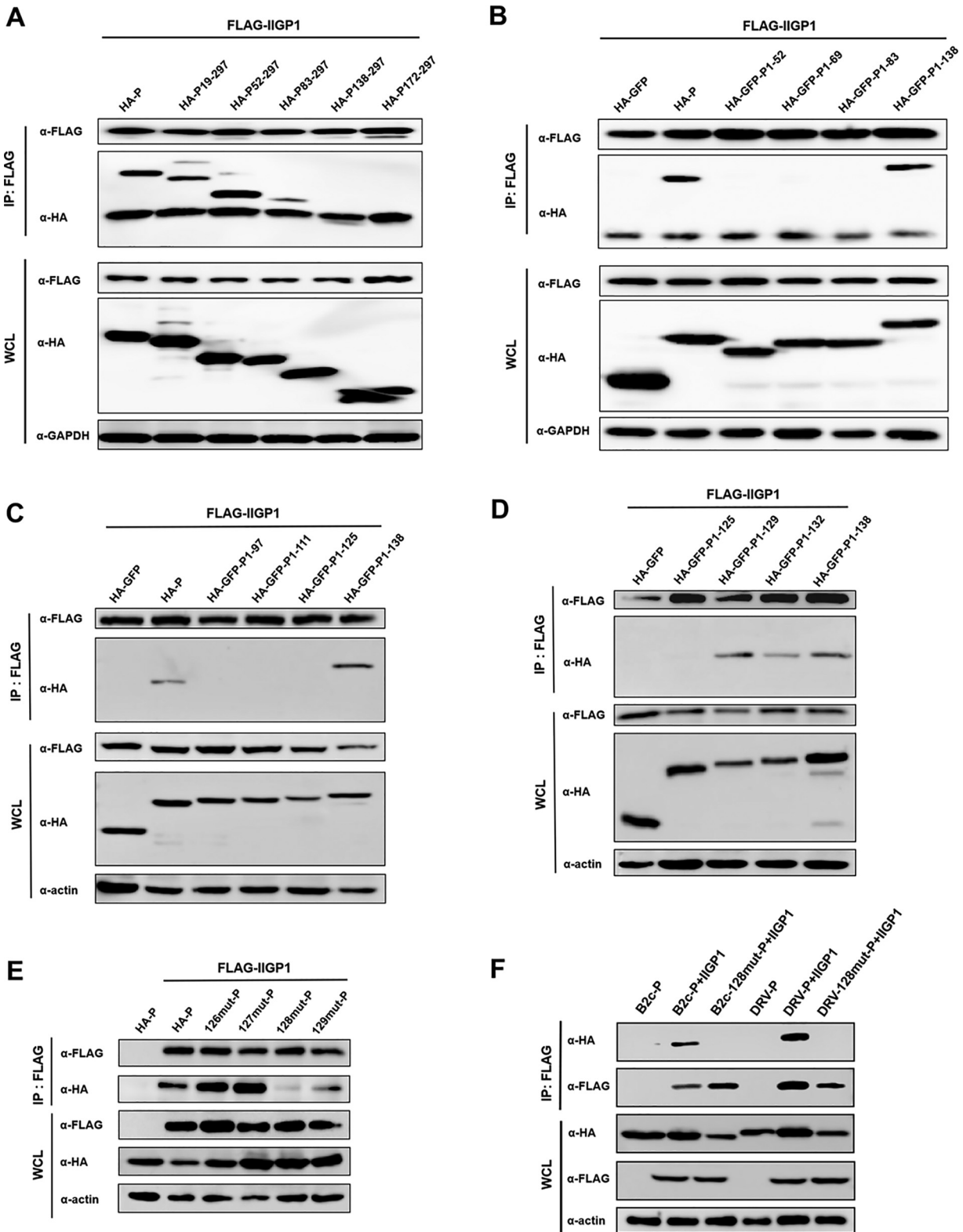
**FIG 7** The Y128 amino acid of RABV-P is critical for its interaction with IIGP1. (A to D) 293T cells were transfected with pC-FLAG-IIGP1, pC-HA-GFP, pC-HA-B2c-P or pCAGGS expressing different HA-B2c-P truncations. At 48 h p.t., co-IP and Western blotting were performed with the indicated antibodies. (E) 293T cells were transfected with pC-FLAG-IIGP1 or pC-HA-B2c-P or pCAGGS expressing different site mutations of HA-B2c-P. At 48 h p.t., co-IP was and Western blotting were performed with the indicated antibodies. (F) 293T cells were transfected with pC-FLAG-IIGP1, pC-HA-B2c-P, pC-HA-DRV-P, or pCAGGS expressing the site mutations of P protein from B2c or DRV. At 48 h p.t., co-IP and Western blotting were performed with the indicated antibodies.
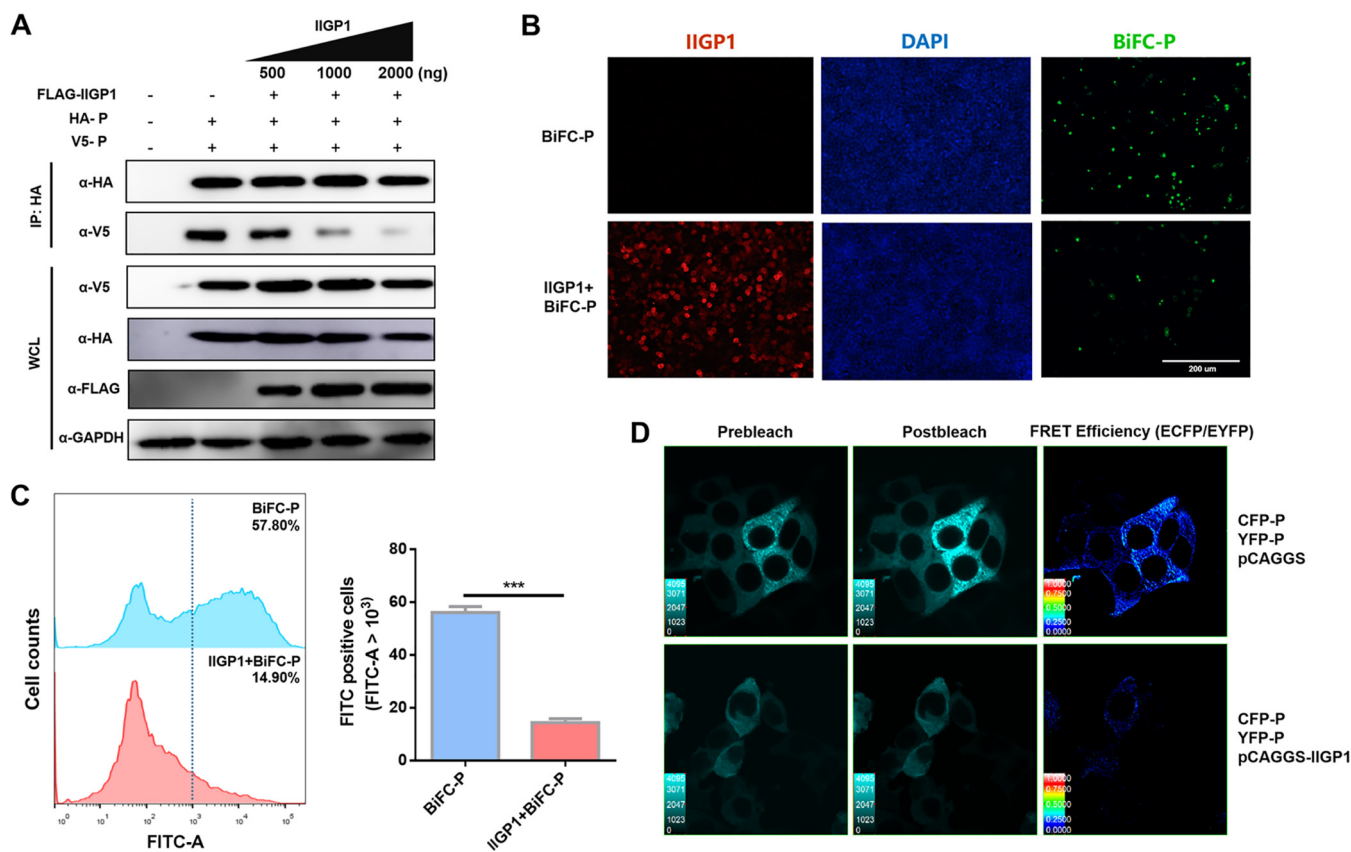
**FIG 8** IIGP1 disrupts the dimerization of RABV-P. (A) 293T cells were transfected with pC-HA-B2c-P, pC-V5-B2c-P, and an increasing amount of pC-FLAG-IIGP1. At 48 h. p.t., cells were lysed and subjected to IP with anti-FLAG tag MAb followed by Western blotting with anti-HA tag or anti-V5 MAbs. (B and C) 293T cells were transfected with pBiFC-VC155-B2c-P together with pBiFC-VN155 (I152L)-B2c-P and pCAGGS, or pBiFC-VC155-B2c-P together with pBiFC-VN155 (I152L)-B2c-P and pC-FLAG-IIGP1. pBiFC-VC155-B2c-P combined with pBiFC-VN155 (I152L)-B2c-P and resulted in BiFC-P, which displays green florescence. At 36 h p.t., cells were fixed and stained by anti-FLAG tag MAb and DAPI, or the cells were harvested for flow cytometry to quantify the FITC fluorescence level in different groups. The scale bar represents 200 $\mu$m. Error bars represent SD. Statistical differences were determined by using Student's $t$ test and are denoted as follows: ***, $P < 0.001$. (D) 293T cells were transfected with pECFP-N1, pEYFP-N1, pECFP-N1 plus pEYFP-N1, pEYFP-N1-P plus pECFP-N1-P, or pEYFP-N1-P plus pECFP-N1-P plus pC-FALG-IIGP1. After 48 h incubation, cells were placed under confocal microscope and analyzed by the FRET procedure. FRET efficiency is shown as dots with different color temperatures.

pC-FLAG-IIGP1 or pCAGGS, were transfected into 293T cells, and then the green fluorescence of fluorescein isothiocyanate (FITC), which indicates P dimerization, was assessed under a fluorescence microscope. As expected, IIGP1 expression obviously decreased the intensity of green fluorescence (Fig. 8B). The intensity of green fluorescence was quantified by flow cytometry, and the results showed that the fluorescence signal of FITC was significantly reduced by IIGP1 expression (Fig. 8C). Alternatively, fluorescence resonance energy transfer (FRET) assay was performed to further confirm that IIGP1 could disrupt P dimerization. FRET efficiency showing P-P interaction was significantly decreased from 0.25 to 0.50 to 0 to 0.25 after IIGP1 expression (Fig. 8D). Together, these data demonstrate that IIGP1 can interfere with P dimerization.

## DISCUSSION

Multiple lines of evidence have shown the antiviral effects of the myxovirus resistance proteins (Mx) and the guanylate-binding proteins (GBPs) among the four families of IFN-inducible GTPases. The two *Mx* gene lineages can restrict distinct spectra of viruses, including influenza virus, human immunodeficiency virus type 1 (HIV-1), vesicular stomatitis virus (VSV), and hepatitis B virus (32–35). Human GBP1 and murine GBP2 were shown to constrain infections of VSV and encephalomyocarditis virus when overexpressed in cell lines (36, 37). Human GBP3 mediated antiviral activity through repression of the polymerase complex of influenza virus, and human GBP5 protein was

able to limit HIV-1 and other retrovirus infections (38). However, there are no reports related to antiviral effects of IRGs and VLIGs. A recent study using transcriptome sequencing (RNA-seq) analysis found that the mRNA levels of GTPase family proteins, including GPB1, GBP2, GBP4, IRGM1, IRGM2, and IIGP1, in RABV-infected mouse brain were upregulated, but their functions during RABV infection were not investigated (39). In our study, by using iTRAQ techniques, we found that four members among the GTPase family proteins, IIGP1, GBP2, GBP4, and GBP5, were upregulated post-RABV infection. Since there is no evidence related to the antiviral effect of IIGP1, we then focused on this GTPase and found that IIGP1 could restrict RABV infection.

Previous studies have shown that IIGP1 plays an important role in protecting the host against intracellular protozoa and bacteria, mainly by translocating to the double-layer membranes and breaking these structures through prenylation (28, 29). A recent study demonstrated that in the murine norovirus model, IRGs' and GBPs' recruitment to the viral replication complex is mediated by the LC3 conjugation system (31). In another study, P and N proteins of measles virus were sufficient to form the cytoplasmic inclusion bodies (40). Most recently, Blondel's group found that Negri bodies (NBs), formed mainly by N and P proteins, were the replication factories in the cytoplasm for RABV, and the dimerization of P protein determines whether NBs can be formed (6). In the present study, we found that IIGP1 directly interacts with RABV P protein and disrupts the dimerization of P protein. Thus, we propose that IIGP1 might be recruited to the area of NBs and thus interfere with the formation of virus particles, which needs to be verified in our future study.

P protein exists as dimers in the cells and forms a complex with soluble nucleoprotein (N0) distributed in the cytosol. This process prevents the newly synthesized N protein from nonspecifically binding to the cell's own RNA and also prevents the N protein from multimerizing (41). The crystal structure data reveal that the amino acids 92 to 131 determine the dimerization of the P protein (12). Yeast two-hybrid experiments confirmed that F114A, W118A, I125A, Y128A, and V129A reduced the dimerization of P protein (42). In this study, we found that IIGP1 can interact with the key amino acids (Y128) for P protein dimerization and thus inhibits viral replication. In another experiment, we attempted to construct a mutant RABV with Y128A, which was supposed to escape the inhibitory effect from IIGP1, but we failed to rescue this recombinant virus. Together, our data confirm that the dimerization of P protein is critical for RBAV replication, providing a potential therapeutic target for RABV.

It is interesting to observe that IIGP1 inhibits RABV infection depending on the infection route. We found that overexpression or deficiency of IIGP1 impacted RABV pathogenicity after i.d. but not i.m. infection. Under different infection routes, RABV may invade into the brain via different pathways. However, the basal and inducible levels of IIGP1 in different parts of the brain may be variable, which may affect viral replication and spread. A previous study showed that the basal and inducible levels of ISG in different neuron cells post-virus infection were quite different. Generally, the basal level of ISG in astrocytes and microglia is obviously higher than that in neurons (43). Another study demonstrated that the basal level of ISG varied between granule cell neurons of the cerebellum and cortical neurons from the cerebral cortex. Some specific ISGs against different neurotropic viruses were expressed more highly in granule cell neurons than those in cortical neurons (44). Thus, the unique innate immune programs of different neuron cells may confer differential susceptibility to neurotropic virus infection. However, the detailed mechanism for the region-specific restriction of viral infection by IIGP1 in mouse brain still needs to be further investigated.

Previous studies suggested that GTPase activity is required for parasite resistance. IIGP1 proteins contain a GTP-binding site, and GDP or GTP binding influences the relocation of IIGP1 in the cells (45). In the presence of GDP, IIGP1 behaves as a monomer, and it oligomerizes after binding with GTP (45). In uninfected IFN-primed cells, IIGP1 is exclusively found in the GDP-bound form and resides in the cytosol or is associated transiently with cell organelles such as the endoplasmic reticulum (46). Once

a cell is infected with IRG-susceptible pathogens such as *T. gondii* or *Chlamydia trachomatis*, the pathogen-containing vacuole (PV) that surrounds these pathogens becomes decorated with GTP-bound IIGP1 (28, 47, 48). GTP binding and the resulting oligomerization of IIGP1 are essential for the association of IIGP1 with PV membranes. IIGP1 has relatively low basal GTPase activity, but it is elevated at higher concentrations of IIGP1. In order to evaluate GTPase activity on the antiviral effect of IIGP1, we constructed a mutant IIGP1, E77A-IIGP1, with lower GTPase activity than WT IIGP1. We found that E77A-IIGP1 still maintained the interaction with P protein, but the antiviral activity of E77A-IIGP1was lower than that of WT IIGP1. Therefore, we propose that the GTPase activity of IIGP1 is associated with its antiviral function, but the detailed mechanisms need to be further investigated in future studies.

In summary, our data provide the first evidence that IIGP1 can restrict viral infection and impede the dimerization of RABV P protein, which provides a basis for further investigation of the role of IIGP1 in inhibiting other viruses. In addition, understanding the importance of the dimerization of P protein for viral assembly provides a potential therapeutic target for RABV.

## MATERIALS AND METHODS

**Cells, viruses, antibodies, and animals.** HEK-293T (human embryonic kidney, 293T), N2a (neuro-blastoma), BV2 (mouse microglioma), and BSR (cloned from BHK-21) cells were cultured in Dulbecco's modified Eagle's medium (DMEM) (Thermo Fisher, USA) supplemented with 10% fetal bovine serum (FBS) (Thermo Fisher, USA). RABV CVS-B2c (B2c) strain (originated from CVS-24 virus by passaging in BHK-21 cells) (49) and WT RABV strain of DRV-Mexico (DRV) (50) were used in the challenge experiments. The monoclonal antibodies (MAb) against FLAG tag, HA tag, V5 tag, and glyceraldehyde-3-phosphate dehydrogenase (GAPDH) were purchased from Medical & Biological Laboratories (MBL, Nagoya, Japan). The MAb against RABV N protein, P protein, and G protein and the polyclonal antibody (pAb) against IIGP1 and purified RABV particles were prepared in our laboratory. The recombinant IFN-$\gamma$ was purchased from Sino Biological (Beijing, China).

The IIGP1 knockout (IIGP1$^{-/-}$) mice of the C57BL/6 background were constructed using the CRISPR/Cas9 system by the Transgenic Animal Facility at Huazhong Agricultural University. The single guide RNA (sgRNA) was designed, and the off-target was tested online (http://crispr.mit.edu/). Two sgRNAs were selected (IIGP1-sgRNA1, GTCACCGGGGAGACGGGATCAGG, and IIGP1-sgRNA2, forward, CCTGCAGGACAT CCGCCTTAACT, and reverse, AGTTAAGGCGGATGTCCTGCAGG) and targeted at exon 3 of the IIGP1 gene and used to construct the knockout mice. The stable IIGP1$^{-/-}$ mice were genotyped by PCR with specific primers (IIGP1-PCR-S, TCTTCCAGTGCCTTTATTGC, and IIGP1-PCR-A, GTCTCCAAATCACTGTCCAA). Female C57BL/6 mice (~6 to 8 weeks old) were obtained from the Hubei Center for Disease Control and housed in the Animal Facility at Huazhong Agricultural University. All experiments involving mice were per-formed following the recommendations in the Guide for the Care and Use of Laboratory Animals of the Ministry of Science and Technology of China and were approved by the Scientific Ethics Committee of Huazhong Agricultural University (permit number HZAUMO-2016-057).

**Screening of upregulated proteins by iTRAQ.** To screen upregulated proteins induced by RABV infection, C57BL/6 mice were infected intracerebrally (i.c.) with B2c at 20 focus-forming units (FFU) or mock infected with the same volume of DMEM. At 6 dpi, mouse brains were harvested and homogenized. Protein expression was analyzed using isobaric tags for relative and absolute quantification (iTRAQ). Briefly, the brain tissues were lysed with trypsin and N termini labeled with tags, and the samples were pooled, fractionated by liquid chromatography, and analyzed by tandem mass spectrometry. The peak area ratio is equivalent to the quantity of each protein, and the upregulated proteins are represented by the relative ratios of the virus-infected group to the mock group.

**Construction and rescue of the recombinant viruses.** The recombinant virus was constructed and rescued as described previously (20). Briefly, murine IIGP1 gene was inserted into the genome of RABV B2c strain between G and L genes by replacing the pseudogene as depicted in Fig. 3A. To rescue the recombinant virus rB2c expressing IIGP1 (rB2c-IIGP1), the plasmid containing the full-length viral genome and the helper plasmids expressing N, P, G, and L proteins were transfected into BSR cells using Lipofectamine 3000 (Thermo Fisher, USA), and rescued virus was harvested at day 4 posttransfection. The rescued virus was propagated and titrated on BSR cells.

**Virus infection and titration.** 293T, N2a, and BV2 cells were infected with rB2c or rB2c-IIGP1 at the indicated MOI for 1 h at 37°C. Cells were washed with phosphate-buffered saline (PBS) three times and cultured in the incubator at 37°C. The cell culture supernatants were collected at indicated time points for virus titration. Virus titers were determined by direct immunofluorescence assay as described previously (20).

**Mouse infection.** Female C57BL/6 mice (6 weeks old) were infected intracranially (i.c.) with 20 $\mu$l of B2c (20 FFU) and mock infected with the same volume of DMEM. At 6 dpi, mice were euthanized with $CO_2$ when moribund and perfused with PBS, and brains were collected for downstream analysis.

Female C57BL/6 mice (8 weeks old) were infected intradermally (i.d.) in both ears with 30 $\mu$l recombinant viruses of rB2c or rB2c-IIGP1 at $3 \times 10^3$ FFU. Body weight changes and mortality of mice were monitored daily. At 6, 9, and 12 dpi, mice were euthanized with $CO_2$, and their brains were collected

for immunohistochemistry, RNA isolation, or qPCR analysis. The mice with body weight loss of more than 25% were euthanized with $CO_2$.

IIGP1-knockout (IIGP1$^{-/-}$) or WT mice (C57BL/6) were infected i.d. with B2c at $1.5 \times 10^3$ FFU, and the clinical signs were monitored daily.

**qPCR.** The brains and cells were subjected to RNA isolation using TRIzol (Invitrogen) according to the manufacturer's instructions, and the qPCR assays were performed as described previously (51). The corresponding primers used for qPCR are as follows: RABV-N, forward, ACACCGCAACTACAAGACA; RABV-N, reverse, ATGGTACTCCAGTTGGCACA; IIGP1, forward, AATACCTGCCTCACGCTCAT; IIGP1, reverse, GCTACTCTGTGGGTTCTGGC; IFN-$\gamma$, forward, GACTGTGATTGCGGGGTTGT; IFN-$\gamma$, reverse, GGCCCGGAGTG TAGACATCT; $\beta$-actin, forward, AGGTGACAGCATTGCTTCTG; and $\beta$-actin, reverse, GCTGCCTCAACACCTC AAC.

To quantify cellular RABV-N RNA levels, total RNA was transcribed using AMV reverse transcriptase XL (TaKaRa, Kusatsu, Japan) and a primer specific for the RABV-N gene. A standard curve was generated from serially diluted plasmids carrying the N gene, and the copy number of N RNA was normalized to 1 $\mu$g of total RNA.

**Immunoprecipitation.** For the immunoprecipitation assay, 293T cells were cotransfected with the mammalian expression vector pCAGGS expressing HA-B2c-P, HA-DRV-P, pV5-B2c-P, FLAG-IIGP1, and/or truncated fragments of HA-B2c-P. At 48 h posttransfection, cells were washed with cold PBS and lysed with NP-40 lysis buffer (50 mM Tris-HCl [pH 7.5], 150 mM NaCl, 5 mM EDTA, and 0.5% NP-40) containing an anti-protease cocktail (Roche) and phenylmethylsulfonyl fluoride (PMSF) (1 mM) for 30 min at 4°C. The cell lysates were centrifuged for 10 min at $12,000 \times g$ at 4°C, and the supernatants were transferred into a new tube and precleared with a Pierce Protein A/G Plus agarose (catalog no. 20424; Thermo Fisher, USA). After being incubated with an MAb against FLAG, HA, or V5 tag for 6 h, the agarose was added into the cell lysates for 1 h at 4°C with rotation. The agaroses were then washed five times with NP-40 lysis buffer, and the bound proteins were analyzed by Western blotting using the indicated antibodies.

**Confocal microscopy.** 293T or N2a cells were seeded on coverslips and transfected with plasmids or infected with B2c. At different time points postinfection, the cells were fixed with 4% paraformaldehyde, permeabilized with 0.1% Triton X-100, and stained with antibodies against HA tag, FLAG tag, RABV-P, IIGP1, or 4′,6-diamidino-2-phenylindole (DAPI).

The infected or mock mice were anesthetized with ketamine-xylazine. Mouse brains were collected and embedded in paraffin. The sections were subsequently stained with antibodies against RABV-N, IIGP1, or DAPI. After being washed, the sections were stained with Alexa 488-conjugated or 594-conjugated secondary antibodies for 1 h at room temperature. Fluorescence was then observed under a Nikon A1 confocal laser microscope system equipped with NIS-Elements imaging software (Nikon, Tokyo, Japan).

**BiFC test.** The full-length P gene from CVS-B2c was inserted into pBiFC-VC155 or pBiFC-VN155 (I152L) vector at EcoRI and KpnI sites, respectively. 293T cells were transfected with pBiFC-VC155-B2c-P, pBiFC-VN155 (I152L)-B2c-P, or pC-FALG-IIGP1. After incubation for 48 h in the dark, cells were fixed with 4% paraformaldehyde (PFA), permeabilized with 0.1% Triton X-100, and stained with antibodies against FLAG tag and DAPI. After being washed, the cells were incubated with Alexa 594-conjugated secondary antibodies for 1 h at room temperature and observed with an Olympus IX51 fluorescence microscope (Olympus, Tokyo, Japan).

**Flow cytometric analysis.** 293T cells in a 12-well plate were transfected with pBiFC-VC155-B2c-P, pBiFC-VN155 (I152L)-B2c-P, pCAGGS, or pC-FLAG-IIGP1. At 36 h posttransfection, cells were digested with trypsin. After being washed twice, single-cell suspensions in PBS (containing 0.2% bovine serum albumin [BSA], wt/vol) were analyzed using a BD FACSVerse (BD Biosciences, USA).

**FRET assay.** The full-length P gene from CVS-B2c was ligated with pECFP-N1 and pEYFP-N1 vector digested by *EcoR I* and *Kpn I*. 293T cells were transfected with (i) pECFP-N1, (ii) pEYFP-N1, (iii) pECFP-N1and pEYFP-N1, (iv) pEYFP-N1-P and pECFP-N1-P, and (v) pEYFP-N1-P, pECFP-N1-P, and pC-FALG-IIGP1. After incubation for 48 h in the dark, the slides with living cells were then moved to the objective table of Zeiss LSM 800 (Zeiss, Jena, Germany). Briefly, images were collected with the multitrack mode. There were two channels in track I. Cyan fluorescent protein (CFP) emission signals were collected through channel I (475 to 525 nm), and FRET emission signals were collected through channel II (530 nm). There was only one channel in track II, and yellow fluorescent protein (YFP) emission signals were collected within this channel (530 nm).

FRET efficiency between CFP and YFP was analyzed using Zeiss LSM software. Crosstalk coefficients were calculated using control cells that expressed only CFP or YFP and expressed as correction factors. Donor coefficients Fd/Dd represent the amount of crosstalk of donor signal into the FRET channel, and Ad/Fd represent the amount of crosstalk of FRET signal into the acceptor channel. Acceptor coefficients Fa/Aa signify the amount of crosstalk of the acceptor signal into the FRET channel, Da/Fa represent the amount of crosstalk of the acceptor signal into the donor channel, and Da/Fa represent the amount of crosstalk of the FRET signal into the donor channel. FRET efficiency was shown as points with different color temperatures.

**Statistical analyses.** Data are expressed as the mean and standard error of the mean. Significant differences were determined by using two-way analysis of variance (ANOVA) and Sidak's multiple-comparison test or Student's *t* tests. The survival ratio was analyzed by log-rank (Mantel-Cox or Gehan-Breslow-Wilcoxon) test. Asterisks in figures indicate statistical significance (*, $P < 0.05$; **, $P < 0.01$; ***, $P < 0.001$).

## REFERENCES

1. Fooks AR, Cliquet F, Finke S, Freuling C, Hemachudha T, Mani RS, Muller T, Nadin-Davis S, Picard-Meyer E, Wilde H, Banyard AC. 2017. Rabies. Nat Rev Dis Primers 3:17091. https://doi.org/10.1038/nrdp.2017.91.

2. Fisher CR, Streicker DG, Schnell MJ. 2018. The spread and evolution of rabies virus: conquering new frontiers. Nat Rev Microbiol 16:241–255. https://doi.org/10.1038/nrmicro.2018.11.

3. Schnell MJ, McGettigan JP, Wirblich C, Papaneri A. 2010. The cell biology of rabies virus: using stealth to reach the brain. Nat Rev Microbiol 8:51–61. https://doi.org/10.1038/nrmicro2260.

4. Hidaka Y, Lim CK, Takayama-Ito M, Park CH, Kimitsuki K, Shiwa N, Inoue KI, Itou T. 2018. Segmentation of the rabies virus genome. Virus Res 252:68–75. https://doi.org/10.1016/j.virusres.2018.05.017.

5. Nikolic J, Le Bars R, Lama Z, Scrima N, Lagaudriere-Gesbert C, Gaudin Y, Blondel D. 2017. Negri bodies are viral factories with properties of liquid organelles. Nat Commun 8:58. https://doi.org/10.1038/s41467-017-00102-9.

6. Lahaye X, Vidy A, Pomier C, Obiang L, Harper F, Gaudin Y, Blondel D. 2009. Functional characterization of Negri bodies (NBs) in rabies virus-infected cells: evidence that NBs are sites of viral transcription and replication. J Virol 83:7948–7958. https://doi.org/10.1128/JVI.00554-09.

7. Albertini AA, Wernimont AK, Muziol T, Ravelli RB, Clapier CR, Schoehn G, Weissenhorn W, Ruigrok RW. 2006. Crystal structure of the rabies virus nucleoprotein-RNA complex. Science 313:360–363. https://doi.org/10.1126/science.1125280.

8. Chenik M, Chebli K, Gaudin Y, Blondel D. 1994. In vivo interaction of rabies virus phosphoprotein (P) and nucleoprotein (N): existence of two N-binding sites on P protein. J Gen Virol 75:2889–2896. https://doi.org/10.1099/0022-1317-75-11-2889.

9. Mavrakis M, Iseni F, Mazza C, Schoehn G, Ebel C, Gentzel M, Franz T, Ruigrok RW. 2003. Isolation and characterisation of the rabies virus N degrees-P complex produced in insect cells. Virology 305:406–414. https://doi.org/10.1006/viro.2002.1748.

10. Mavrakis M, McCarthy AA, Roche S, Blondel D, Ruigrok RW. 2004. Structure and function of the C-terminal domain of the polymerase cofactor of rabies virus. J Mol Biol 343:819–831. https://doi.org/10.1016/j.jmb.2004.08.071.

11. Chenik M, Schnell M, Conzelmann KK, Blondel D. 1998. Mapping the interacting domains between the rabies virus polymerase and phosphoprotein. J Virol 72:1925–1930. https://doi.org/10.1128/JVI.72.3.1925-1930.1998.

12. Ivanov I, Crepin T, Jamin M, Ruigrok RW. 2010. Structure of the dimerization domain of the rabies virus phosphoprotein. J Virol 84:3707–3710. https://doi.org/10.1128/JVI.02557-09.

13. Bauer A, Nolden T, Nemitz S, Perlson E, Finke S. 2015. A dynein light chain 1 binding motif in rabies virus polymerase L protein plays a role in microtubule reorganization and viral primary transcription. J Virol 89:9591–9600. https://doi.org/10.1128/JVI.01298-15.

14. Raux H, Flamand A, Blondel D. 2000. Interaction of the rabies virus P protein with the LC8 dynein light chain. J Virol 74:10212–10216. https://doi.org/10.1128/jvi.74.21.10212-10216.2000.

15. Li Y, Dong W, Shi Y, Deng F, Chen X, Wan C, Zhou M, Zhao L, Fu ZF, Peng G. 2016. Rabies virus phosphoprotein interacts with ribosomal protein L9 and affects rabies virus replication. Virology 488:216–224. https://doi.org/10.1016/j.virol.2015.11.018.

16. Takeuchi O, Akira S. 2010. Pattern recognition receptors and inflammation. Cell 140:805–820. https://doi.org/10.1016/j.cell.2010.01.022.

17. Schoggins JW, Rice CM. 2011. Interferon-stimulated genes and their antiviral effector functions. Curr Opin Virol 1:519–525. https://doi.org/10.1016/j.coviro.2011.10.008.

18. Blondel D, Regad T, Poisson N, Pavie B, Harper F, Pandolfi PP, De Thé H, Chelbi-Alix MK. 2002. Rabies virus P and small P products interact directly with PML and reorganize PML nuclear bodies. Oncogene 21:7957–7970. https://doi.org/10.1038/sj.onc.1205931.

19. Davis BM, Fensterl V, Lawrence TM, Hudacek AW, Sen GC, Schnell MJ. 2017. Ifit2 is a restriction factor in rabies virus pathogenicity. J Virol 91. https://doi.org/10.1128/JVI.00889-17.

20. Tian D, Luo Z, Zhou M, Li M, Yu L, Wang C, Yuan J, Li F, Tian B, Sui B, Chen H, Fu ZF, Zhao L. 2016. Critical role of K1685 and K1829 in the large protein of rabies virus in viral pathogenicity and immune evasion. J Virol 90:232–244. https://doi.org/10.1128/JVI.02050-15.

21. Tang HB, Lu ZL, Wei XK, Zhong TZ, Zhong YZ, Ouyang LX, Luo Y, Xing XW, Liao F, Peng KK, Deng CQ, Minamoto N, Luo TR. 2016. Viperin inhibits rabies virus replication via reduced cholesterol and sphingomyelin and is regulated upstream by TLR4. Sci Rep 6:30529. https://doi.org/10.1038/srep30529.

22. Yuan Y, Wang Z, Tian B, Zhou M, Fu ZF, Zhao L. 2019. Cholesterol 25-hydroxylase suppresses rabies virus infection by inhibiting viral entry. Arch Virol 164:2963–2974. https://doi.org/10.1007/s00705-019-04415-6.

23. Pilla-Moffett D, Barber MF, Taylor GA, Coers J. 2016. Interferon-inducible GTPases in host resistance, inflammation and disease. J Mol Biol 428:3495–3513. https://doi.org/10.1016/j.jmb.2016.04.032.

24. Seixas E, Escrevente C, Seabra MC, Barral DC. 2018. Rab GTPase regulation of bacteria and protozoa phagocytosis occurs through the modulation of phagocytic receptor surface expression. Sci Rep 8:12998. https://doi.org/10.1038/s41598-018-31171-5.

25. Martens S, Sabel K, Lange R, Uthaiah R, Wolf E, Howard JC. 2004. Mechanisms regulating the positioning of mouse p47 resistance GTPases LRG-47 and IIGP1 on cellular membranes: retargeting to plasma membrane induced by phagocytosis. J Immunol 173:2594–2606. https://doi.org/10.4049/jimmunol.173.4.2594.

26. Uthaiah RC, Praefcke GJ, Howard JC, Herrmann C. 2003. IIGP1, an interferon-gamma-inducible 47-kDa GTPase of the mouse, showing cooperative enzymatic activity and GTP-dependent multimerization. J Biol Chem 278:29336–29343. https://doi.org/10.1074/jbc.M211973200.

27. Ghosh A, Uthaiah R, Howard J, Herrmann C, Wolf E. 2004. Crystal structure of IIGP1: a paradigm for interferon-inducible p47 resistance GTPases. Mol Cell 15:727–739. https://doi.org/10.1016/j.molcel.2004.07.017.

28. Martens S, Parvanova I, Zerrahn J, Griffiths G, Schell G, Reichmann G, Howard JC. 2005. Disruption of Toxoplasma gondii parasitophorous vacuoles by the mouse p47-resistance GTPases. PLoS Pathog 1:e24. https://doi.org/10.1371/journal.ppat.0010024.

29. Ferreira-da-Silva M. d F, da Fonseca Ferreira-da-Silva M, Springer-Frauenhoff HM, Bohne W, Howard JC. 2014. Identification of the microsporidian Encephalitozoon cuniculi as a new target of the IFNgamma-inducible IRG resistance system. PLoS Pathog 10:e1004449. https://doi.org/10.1371/journal.ppat.1004449.

30. Liesenfeld O, Parvanova I, Zerrahn J, Han SJ, Heinrich F, Munoz M, Kaiser F, Aebischer T, Buch T, Waisman A, Reichmann G, Utermohlen O, von Stebut E, von Loewenich FD, Bogdan C, Specht S, Saeftel M, Hoerauf A, Mota MM, Konen-Waisman S, Kaufmann SH, Howard JC. 2011. The IFN-gamma-inducible GTPase, Irga6, protects mice against Toxoplasma gondii but not against Plasmodium berghei and some other intracellular pathogens. PLoS One 6:e20568. https://doi.org/10.1371/journal.pone.0020568.

31. Biering SB, Choi J, Halstrom RA, Brown HM, Beatty WL, Lee S, McCune BT, Dominici E, Williams LE, Orchard RC, Wilen CB, Yamamoto M, Coers J, Taylor GA, Hwang S. 2017. Viral replication complexes are targeted by LC3-guided interferon-inducible GTPases. Cell Host Microbe 22:74–85.e7. https://doi.org/10.1016/j.chom.2017.06.005.

32. Busnadiego I, Kane M, Rihn SJ, Preugschas HF, Hughes J, Blanco-Melo D, Strouvelle VP, Zang TM, Willett BJ, Boutell C, Bieniasz PD, Wilson SJ. 2014. Host and viral determinants of Mx2 antiretroviral activity. J Virol 88:7738–7752. https://doi.org/10.1128/JVI.00214-14.

33. Maarifi G, Hannoun Z, Geoffroy MC, El Asmi F, Zarrouk K, Nisole S, Blondel D, Chelbi-Alix MK. 2016. MxA mediates SUMO-induced resis-

tance to vesicular stomatitis virus. J Virol 90:6598–6610. https://doi.org/10.1128/JVI.00722-16.

34. Liu Z, Pan Q, Ding S, Qian J, Xu F, Zhou J, Cen S, Guo F, Liang C. 2013. The interferon-inducible MxB protein inhibits HIV-1 infection. Cell Host Microbe 14:398–410. https://doi.org/10.1016/j.chom.2013.08.015.

35. Pavlovic J, Haller O, Staeheli P. 1992. Human and mouse Mx proteins inhibit different steps of the influenza virus multiplication cycle. J Virol 66:2564–2569. https://doi.org/10.1128/JVI.66.4.2564-2569.1992.

36. Carter CC, Gorbacheva VY, Vestal DJ. 2005. Inhibition of VSV and EMCV replication by the interferon-induced GTPase, mGBP-2: differential requirement for wild-type GTP binding domain. Arch Virol 150:1213–1220. https://doi.org/10.1007/s00705-004-0489-2.

37. Anderson SL, Carton JM, Lou J, Xing L, Rubin BY. 1999. Interferon-induced guanylate binding protein-1 (GBP-1) mediates an antiviral effect against vesicular stomatitis virus and encephalomyocarditis virus. Virology 256:8–14. https://doi.org/10.1006/viro.1999.9614.

38. Nordmann A, Wixler L, Boergeling Y, Wixler V, Ludwig S. 2012. A new splice variant of the human guanylate-binding protein 3 mediates anti-influenza activity through inhibition of viral transcription and replication. FASEB J 26:1290–1300. https://doi.org/10.1096/fj.11-189886.

39. Li L, Wang H, Jin H, Cao Z, Feng N, Zhao Y, Zheng X, Wang J, Li Q, Zhao G, Yan F, Wang L, Wang T, Gao Y, Tu C, Yang S, Xia X. 2016. Interferon-inducible GTPase: a novel viral response protein involved in rabies virus infection. Arch Virol 161:1285–1293. https://doi.org/10.1007/s00705-016-2795-x.

40. Zhou Y, Su JM, Samuel CE, Ma D. 2019. Measles virus forms inclusion bodies with properties of liquid organelles. J Virol 93:e00948-19. https://doi.org/10.1128/JVI.00948-19.

41. Mavrakis M, Mehouas S, Real E, Iseni F, Blondel D, Tordo N, Ruigrok RW. 2006. Rabies virus chaperone: identification of the phosphoprotein peptide that keeps nucleoprotein soluble and free from non-specific RNA. Virology 349:422–429. https://doi.org/10.1016/j.virol.2006.01.030.

42. Gerard FC, Ribeiro Ede A, Jr, Leyrat C, Ivanov I, Blondel D, Longhi S, Ruigrok RW, Jamin M. 2009. Modular organization of rabies virus phosphoprotein. J Mol Biol 388:978–996. https://doi.org/10.1016/j.jmb.2009.03.061.

43. Zhao L, Rose KM, Elliott R, Van Rooijen N, Weiss SR. 2011. Cell-type-specific type I interferon antagonism influences organ tropism of murine coronavirus. J Virol 85:10058–10068. https://doi.org/10.1128/JVI.05075-11.

44. Cho H, Proll SC, Szretter KJ, Katze MG, Gale M, Jr, Diamond MS. 2013. Differential innate immune response programs in neuronal subtypes determine susceptibility to infection in the brain by positive-stranded RNA viruses. Nat Med 19:458–464. https://doi.org/10.1038/nm.3108.

45. Papic N, Hunn JP, Pawlowski N, Zerrahn J, Howard JC. 2008. Inactive and active states of the interferon-inducible resistance GTPase, Irga6, in vivo. J Biol Chem 283:32143–32151. https://doi.org/10.1074/jbc.M804846200.

46. Hunn JP, Koenen-Waisman S, Papic N, Schroeder N, Pawlowski N, Lange R, Kaiser F, Zerrahn J, Martens S, Howard JC. 2008. Regulatory interactions between IRG resistance GTPases in the cellular response to Toxoplasma gondii. EMBO J 27:2495–2509. https://doi.org/10.1038/emboj.2008.176.

47. Coers J, Bernstein-Hanley I, Grotsky D, Parvanova I, Howard JC, Taylor GA, Dietrich WF, Starnbach MN. 2008. Chlamydia muridarum evades growth restriction by the IFN-gamma-inducible host resistance factor Irgb10. J Immunol 180:6237–6245. https://doi.org/10.4049/jimmunol.180.9.6237.

48. Haldar AK, Saka HA, Piro AS, Dunn JD, Henry SC, Taylor GA, Frickel EM, Valdivia RH, Coers J. 2013. IRG and GBP host resistance factors target aberrant, "non-self" vacuoles characterized by the missing of "self" IRGM proteins. PLoS Pathog 9:e1003414. https://doi.org/10.1371/journal.ppat.1003414.

49. Wang ZW, Sarmento L, Wang Y, Li XQ, Dhingra V, Tseggai T, Jiang B, Fu ZF. 2005. Attenuated rabies virus activates, while pathogenic rabies virus evades, the host innate immune responses in the central nervous system. J Virol 79:12554–12565. https://doi.org/10.1128/JVI.79.19.12554-12565.2005.

50. Zhang G, Fu ZF. 2012. Complete genome sequence of a street rabies virus from Mexico. J Virol 86:10892–10893. https://doi.org/10.1128/JVI.01778-12.

51. Tian B, Zhou M, Yang Y, Yu L, Luo Z, Tian D, Wang K, Cui M, Chen H, Fu ZF, Zhao L. 2017. Lab-attenuated rabies virus causes abortive infection and induces cytokine expression in astrocytes by activating mitochondrial antiviral-signaling protein signaling pathway. Front Immunol 8:2011. https://doi.org/10.3389/fimmu.2017.02011.